JOURNAL OF GEOPHYSICAL RESEARCH, VOL. 113, B12307, doi:10.1029/2008JB005733, 2008

A two-dimensional hybrid method for modeling seismic wave propagation in anisotropic media

Liang Zhao,[1] Lianxing Wen,[2] Ling Chen,[1] and Tianyu Zheng[1]

Received 3 April 2008; revised 12 September 2008; accepted 9 October 2008; published 25 December 2008.

[1] A hybrid method is developed for calculating synthetic seismograms for seismic waves propagating in two-dimensional localized heterogeneous anisotropic media. The hybrid method is a combination of analytic and numerical methods, with the numerical method (finite difference, or FD) applied in the heterogeneous anisotropic region only and the analytic method (generalized ray theory, or GRT) outside. The GRT solutions from a seismic source are interfaced with the FD calculation at the boundaries of the anisotropic region; and seismic responses at the Earth's surface are obtained from the output of FD calculation. Synthetic experiments on both isotropic and anisotropic models demonstrate the validity of the new method in simulating seismic wave propagation in complex media. We applied the hybrid method to study the SKS wave propagation in the upper mantle. We calculated the synthetics for a series of laterally varying anisotropic models, including a layer with varying anisotropy, two-layer anisotropy, separated anisotropic body and those may be related to subduction zones. For these laterally varying models, SKS waveforms exhibit higher sensitivity to the spatial variation of anisotropy than the shear wave splitting parameters do. The results of this study demonstrate the potential of the proposed hybrid method for high-resolution imaging the laterally varying anisotropic structures from seismological observations, when the tectonic structures can be approximated as two-dimensional.

Citation: Zhao, L., L. Wen, L. Chen, and T. Zheng (2008), A two-dimensional hybrid method for modeling seismic wave propagation in anisotropic media, *J. Geophys. Res.*, *113*, B12307, doi:10.1029/2008JB005733.

1. Introduction

[2] The origin of seismic anisotropy is of fundamental importance to the understanding of the lattice-preferred orientation (LPO) of mantle minerals and mantle flow that produces it. The LPO of anisotropic olivine crystals in the upper mantle is believed to be the primary cause for SKS wave splitting [*Savage*, 1999; *Mainprice et al.*, 2000], although alignments of mantle minerals in some region of the lowermost mantle also contribute it [*Niu and Perez*, 2004; *Wang and Wen*, 2007]. Laboratory studies show that under moderate to large strains and dry conditions, the *a* axis of olivine crystals become aligned in the direction of maximum finite extension [*Karato*, 1987] or in the direction of mantle flow [*Zhang and Karato*, 1995].

[3] In recent decades, seismic anisotropy analyses, such as shear wave splitting measurements [*Vinnik et al.*, 1989; *Silver and Chan*, 1991; *Savage*, 1999] or multichannel analysis [*Chevrot*, 2000], have found wide applications in inferring the deformation in the upper mantle. Most of the studies are based upon the particle motion analysis by assuming that the seismic wave propagates through a single or several laterally homogeneous anisotropic layers [*Silver and Savage*, 1994]. Such analyses yield two splitting parameters: fast polarization direction ϕ and delay time between the fast and slow directions δt. In recent years, many seismic studies showed evidence of rapid lateral variations of splitting parameters over distances of less than 50 km, such as, in the regions of the San Andreas Fault [*Hartog and Schwartz*, 2000], central Tibet [*Huang et al.*, 2000], north China [*Zhao and Zheng*, 2005], and northern Apennines [*Salimbeni et al.*, 2007]. Such inferred rapid variations call into question of the validity of the assumptions in the shear wave splitting analyses. Full wave calculations of synthetic seismograms are needed to validate the results from those analyses. The ability to simulate wave propagation in a complex anisotropic medium would also allow observed waveform features to be analyzed and yield more detailed anisotropy information than the splitting parameters ϕ and δt. This indicates a demand for new techniques capable of modeling seismic wave propagation through laterally varying anisotropic structures.

[4] Several seismic methods, including both analytic and numerical ones, have been developed to simulate the wave propagation through anisotropic structures. However, both analytical and numerical methods have difficulties in forward synthetic calculations for seismic propagation in laterally varying anisotropic structures. The analytic methods [e.g., *Keith and Crampin*, 1977a, 1977b; *Booth and Crampin*, 1983; *Saltzer et al.*, 2000] were limited to one-dimensional

[1] Seismological Laboratory, Institute of Geology and Geophysics, Chinese Academy of Sciences, Beijing, China.
[2] Department of Geosciences, State University of New York at Stony Brook, Stony Brook, New York, USA.

0148-0227/08/2008JB005733$09.00

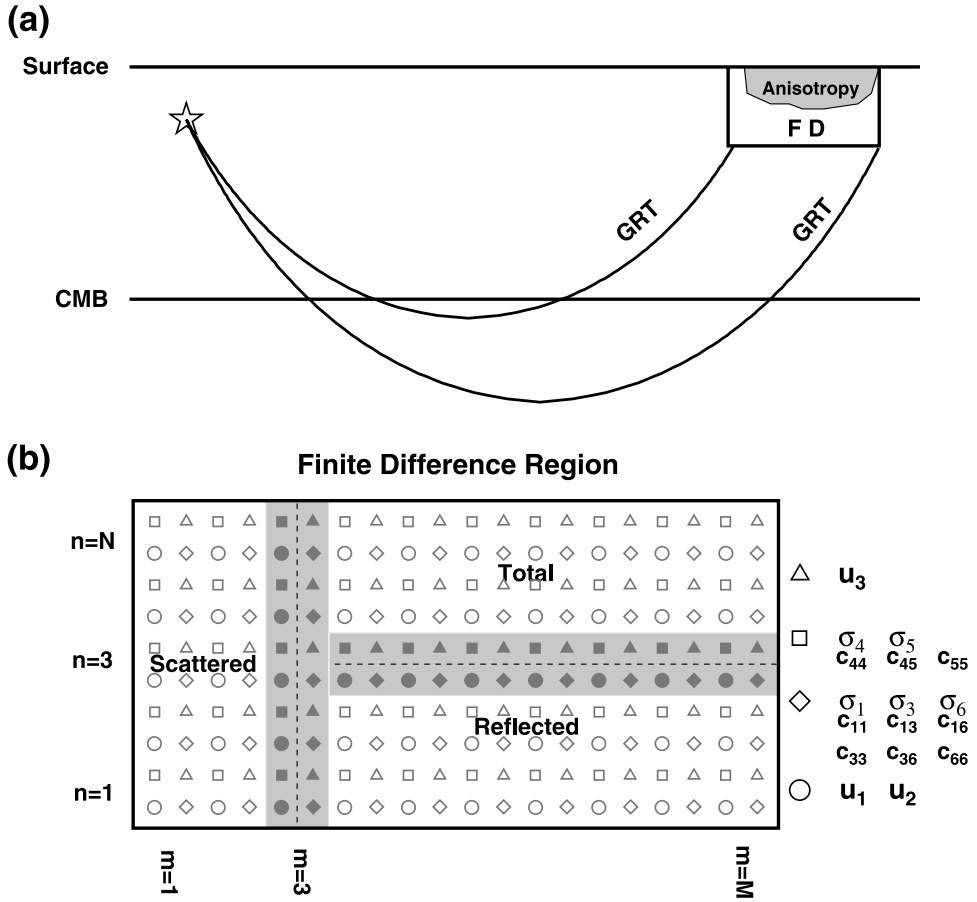

Figure 1. (a) Schematic illustration of interfacing of the hybrid method. The lateral varying anisotropic regions are assumed to be confined inside the small box, where the finite difference technique is applied. Generalized ray theory (GRT) is used to calculate wave propagation from the source to the bottom of the finite difference (FD) region. (b) Division of the finite difference region. The FD region is divided into three parts, where different wavefields are calculated [*Wen and Helmberger*, 1998a] (see text and auxiliary material for details).

anisotropic layers and therefore not applicable for laterally varying structures. On the other hand, numerical methods, such as finite difference (FD) or spectral element, can handle heterogeneous anisotropic structures, but they [e.g., *Igel et al.*, 1995; *Komatitsch et al.*, 2000; *Yang et al.*, 2002] are computationally expensive (especially for simulating teleseismic wave propagation) and have been limited to applications to small-scale models or low-frequency simulations. To deal with heterogeneous anisotropic media, some studies [e.g., *Ryberg et al.*, 2000; *Rümpker and Ryberg*, 2000; *Rümpker et al.*, 2003; *Chevrot et al.*, 2004] assumed that a plane horizontal shear wavefront enters the numerical calculation region from an underlying isotropic layer. In those cases, the effects of wavefront curvature and point source properties were not taken into account, which may introduce artifacts to the synthetic seismograms.

[5] *Wen and Helmberger* [1998a] and *Wen* [2002] proposed effective P-SV and SH hybrid methods for synthetic modeling involving localized heterogeneous isotropic structures near the core-mantle boundary. These methods are combination of both analytical and numerical methods with the numerical calculations limited in the localized heterogeneous regions. The hybrid methods have been applied to investigate the structural heterogeneity in the lowermost mantle and the core [e.g., *Wen and Helmberger*, 1998a, 1998b; *Wen*, 2002; *Wen and Niu*, 2002] and were recently adopted to study the lithospheric and upper mantle structures [*Chen et al.*, 2005]. In this study, we propose a two-dimensional hybrid method to simulate seismic wave propagation through laterally varying anisotropic structures. This method is suited for studying seismic anisotropy when the tectonic structures are approximately two-dimensional with the symmetry axis approximately perpendicular to the great circle plane of the wave propagation, i.e., the anisotropic structures are invariant in the direction perpendicular to the great circle plane [e.g., *Long et al.*, 2008]. We present the theory of the hybrid method in section 2, the validity test of the method in section 3, and synthetic calculations for various anisotropic models and discussions in section 4.

2. A Two-Dimensional Hybrid Method for Calculating Synthetic Seismograms for Wave Propagation in a Heterogeneous Anisotropic Medium

[6] The concept of our hybrid method is illustrated in Figure 1a [*Zhao et al.*, 2006]. The calculation consists of three

parts including the generalized ray theory (GRT), GRT-FD interfacing and FD, following *Wen and Helmberger* [1998a]. We assume that the laterally varying anisotropic medium is localized and is within a box in which a FD technique is applied. The GRT [*Helmberger*, 1983] is used to calculate source excitation and wave propagation from the source to the FD region, and the GRT solutions are interfaced with the FD calculation in the shaded regions in Figure 1b. The synthetics at the surface of the Earth are obtained at the top grid points of FD calculations. The Earth flattening approximation is adopted in these calculations.

2.1. Two-Dimensional FD Method for Elastic Wave Propagation

[7] The FD modeling is performed in a two-dimensional Cartesian coordinate system (x_1–x_3), in which x_1 and x_3 are the horizontal and vertical axis, respectively. Assuming that material properties and wavefields are invariant in x_2 direction and a line source, the two-dimensional elastic wave equations are described as [e.g., *Ryberg et al.*, 2000]

$$\begin{aligned}\rho\frac{\partial^2 u_1}{\partial t^2} &= \sigma_{1,1} + \sigma_{5,3}\\ \rho\frac{\partial^2 u_2}{\partial t^2} &= \sigma_{6,1} + \sigma_{4,3},\\ \rho\frac{\partial^2 u_3}{\partial t^2} &= \sigma_{5,1} + \sigma_{3,3}\end{aligned} \tag{1}$$

where u_i and $\partial^2 u_i/\partial t^2$ denote the ith component of displacement and acceleration at (x, z, t), σ_i ($i = 1, 6$) represent the six independent stress components [σ_{11},σ_{22},σ_{33},σ_{23},σ_{13},σ_{12}], respectively, a comma in the lower index $\sigma_{i,j}$ represents derivatives $\partial\sigma_i/\partial x_j$, ρ (x) denotes the density. The stress tensor σ_i can be given by stress-strain relation or the generalized Hooke's law in (x_1–x_3) system represented as

$$\sigma_i = c_{i1}u_{1,1} + c_{i3}u_{3,3} + c_{i4}u_{2,3} + c_{i5}(u_{3,1} + u_{1,3}) + c_{i6}u_{2,1}, \tag{2}$$

where the stiffness tensor is represented in a two-index notation c_{ij} [*Musgrave*, 1970].

[8] We extended the staggered grid scheme by *Virieux* [1984, 1986] to finite differencing the two-dimensional elastic wave equations for an anisotropic medium. Finite difference grids are illustrated in Figure 1b, where vertical velocity is indicated by triangles, horizontal and tangential velocities are represented by circles, and the stresses are marked by diamonds and squares, respectively. Using v_i replaces velocity $\partial u/\partial t$, and then the equations (1) and (2) are transformed into a first-order hyperbolic system

$$\begin{aligned}\rho\frac{\partial v_1}{\partial t} &= \sigma_{1,1} + \sigma_{5,3},\\ \rho\frac{\partial v_2}{\partial t} &= \sigma_{6,1} + \sigma_{4,3},\\ \rho\frac{\partial v_3}{\partial t} &= \sigma_{5,1} + \sigma_{3,3},\end{aligned} \tag{3}$$

$$\frac{\partial\sigma_i}{\partial t} = c_{i1}\frac{\partial v_{1,1}}{\partial t} + c_{i3}\frac{\partial v_{3,3}}{\partial t} + c_{i4}\frac{\partial v_{2,3}}{\partial t} + c_{i5}\left(\frac{\partial v_{3,1}}{\partial t} + \frac{\partial v_{1,3}}{\partial t}\right) + c_{i6}\frac{\partial v_{2,1}}{\partial t}. \tag{4}$$

With the anisotropy characterized by nine independent elastic constants [*Musgrave*, 1970], equation (4) could be described as

$$\begin{aligned}\frac{\partial\sigma_1}{\partial t} &= c_{11}\frac{\partial v_{1,1}}{\partial t} + c_{13}\frac{\partial v_{3,3}}{\partial t} + c_{16}\frac{\partial v_{2,1}}{\partial t},\\ \frac{\partial\sigma_3}{\partial t} &= c_{31}\frac{\partial v_{1,1}}{\partial t} + c_{33}\frac{\partial v_{3,3}}{\partial t} + c_{36}\frac{\partial v_{2,1}}{\partial t},\\ \frac{\partial\sigma_4}{\partial t} &= c_{44}\frac{\partial v_{2,3}}{\partial t} + c_{45}\left(\frac{\partial v_{3,1}}{\partial t} + \frac{\partial v_{1,3}}{\partial t}\right),\\ \frac{\partial\sigma_5}{\partial t} &= c_{54}\frac{\partial v_{2,3}}{\partial t} + c_{55}\left(\frac{\partial v_{3,1}}{\partial t} + \frac{\partial v_{1,3}}{\partial t}\right),\\ \frac{\partial\sigma_6}{\partial t} &= c_{61}\frac{\partial v_{1,1}}{\partial t} + c_{63}\frac{\partial v_{3,3}}{\partial t} + c_{66}\frac{\partial v_{2,1}}{\partial t}.\end{aligned} \tag{5}$$

Absorbing boundary conditions [*Clayton and Engquist*, 1977] are applied at the left, right, and bottom boundaries of the FD region, and free-surface boundary conditions are applied at the top boundary of the FD region.

2.2. GRT-FD Interfacing and GRT Calculation

[9] We followed the approach by *Wen and Helmberger* [1998a] to deal with GRT-FD interfacing and GRT, except that our FD region is characterized by anisotropic structures. We briefly review the technique in this section. Readers are referred to *Wen and Helmberger* [1998a] for the details of the method. For the GRT-FD interfacing, the FD region is partitioned to three subregions named as scattered, reflected, and total regions, respectively, separated by the dashed lines in Figure 1b. In the total region, the whole wavefield is calculated and the heterogeneous anisotropic structure is only present in this region. In the reflected region, the reflection from the anisotropic region (i.e., energy propagating downward) is taken into account and the reflection wavefields are calculated. In the scattered region, the leftward propagating energy is considered, and then the scattered field is calculated. For a one-dimensional model, the scattered energy is zero [*Wen and Helmberger*, 1998a]. The explicit finite difference formulations in these special regions are presented in the auxiliary material.[1]

[10] Let the incident wavefield be I_0, the one-dimensional solution of the wavefield be T_0, the reflected wavefield due to the one-dimensional model be R_0, the total wavefield be T, the reflected wavefield be R, and the scattered wavefield be S. Here, I, T, R, and S are either velocity (v_1,v_2,v_3) or stresses (σ_1,σ_3,σ_4,σ_5,σ_6). There are general relationships among S, I, T, and R, namely [*Wen and Helmberger*, 1998a],

$$\begin{aligned}T &= I_0 + R \quad or \quad R = T - I_0,\\ S &= T - T_0 \quad or \quad T = S + T_0,\\ S &= R - R_0 \quad or \quad R = S + R_0.\end{aligned} \tag{6}$$

The finite difference schemes are applied directly in those regions since wavefields in those regions satisfy the wave equations individually. In the interiors of the FD region, the explicit schemes of fourth order [e.g., *Levander*, 1988] in space and second order in time are applied, whereas those of second order in space and time are used for the grid points indicated by solid symbols in Figure 1b.

[1] Auxiliary materials are available in the HTML. doi:10.1029/2008JB005733.

[11] To correct the line source response, the point source solution can be obtained by relationship [e.g., *Stead and Helmberger*, 1988] as

$$v_{point} = \frac{2}{\sqrt{R}+\sqrt{x}} \frac{1}{\sqrt{t}} * \frac{d}{dt} v_{line}, \quad (7)$$

where R and x are the total and horizontal distance, respectively.

3. Validation and Comparisons With Other Methods

[12] In this section, we check the validity of our new hybrid method through comparing synthetics of different methods for SKS wave incidence at distances greater than 80°. Our benchmarks include models with one- and two-dimensional isotropic media and one-dimensional anisotropic media. We also test the results of the routine methodology of shear wave splitting measurement by *Silver and Chan* [1991] (the "SC method" for brevity hereafter) for models with a single anisotropic layer.

3.1. Isotropic Models

[13] For one-dimensional isotropic media, we used the isotropic one-dimensional Preliminary Reference Earth Model (PREM) [*Dziewonski and Anderson*, 1981] and tested our method against GRT. SKS horizontal velocities calculated by the new hybrid method and those by GRT [*Helmberger*, 1983] show an excellent agreement in terms of both waveshape and absolute amplitude (Figure 2). Figure 2b (left) shows a comparison of synthetics for receivers marked by triangles and Figure 2b (right) shows for receivers marked by squares in Figure 2a.

[14] For two-dimensional isotropic media, we designed a laterally varying heterogeneous isotropic model (Figure 3a) embedded in the PREM [*Dziewonski and Anderson*, 1981] and tested against the hybrid P-SV method developed by *Wen and Helmberger* [1998a]. The horizontal and vertical velocities from the two calculations show an excellent agreement in both waveshape and absolute amplitude (Figure 3b). Moreover, the tangential component of velocity exhibits nearly zero energy relative to the radial and vertical components as what would be expected for the isotropic structures. This agreement demonstrates the validity of the new hybrid method for calculating synthetics in laterally varying isotropic models.

3.2. Layered Anisotropic Models

[15] For layered anisotropic media, we designed a series of models using the elastic constants of a transversely anisotropic medium that possesses 6.59% anisotropy of shear waves for the vertical plane wave propagation (Table 1) [*Keith and Crampin*, 1977b] and tested against the one-dimensional reflectivity method developed by *Keith and Crampin* [1977a, 1977b]. Our model is characterized by a single anisotropic layer (with a thickness of 111 km in the example) confined within the shallow depth of the PREM (Figure 4a). The incident plane of the seismic waves corresponds to the east vertical plane. Unless indicated otherwise, we refer hereafter the x_1, x_2, and x_3 axes to be the east (radial), north (tangential), and upward vertical directions of the geographic coordinate system, respectively.

[16] A ray parameter of 5.6s/deg is used in the one-dimensional reflectivity method computation as an approximation to that of the SKS phases in the hybrid method calculations. The results from the reflectivity method calculations are convolved with the same SKS phase as that used in the GRT-FD interface of the hybrid method. Figure 4b shows a comparison of the synthetics calculated on the basis of the two methods for models with fast directions of N30°E and N150°E, respectively. The horizontal and vertical velocities calculated on the basis of the two methods show an excellent agreement in both waveshape and amplitude (Figure 4b).

3.3. Comparison With the SC Method for Models With a Single Anisotropic Layer

[17] Different orientations of the anisotropy are examined by rotating the *a* axis of the anisotropic medium clockwise from 0° to 180° with respect to north with an increment of 15°. Figure 5a shows horizontal components of surface motions at an epicenter distance 88.83° for models with varying *a* axis orientations. The top, middle and bottom traces of the horizontal components are for incident planes parallel or perpendicular to the *a* axis of the anisotropic structure. Only for such incident planes, the incident SKS wave does not generate any tangential motion. For the cases of other incident plane, the anisotropy produces SKS arrivals on the tangential component.

[18] It is interesting to note that a broadened phase is recognized in x_1 (radial) components, and the waveform changes with the fast direction of media (Figure 5a). We can explain the broadened phase with an energy projection sketch (Figure 6). After an SKS wave propagates through an anisotropic medium, the incident wave is split into orthogonal fast and slow components. In x_1 axis, the projections of the fast and slow components introduce double phases, while the amplitudes and polarity of the double phases are functions of the angles between x_1 axis and the fast component, respectively. If the delay time between the fast and the slow components is greater than 1/4 period of the incident phase, the two projections separate the energy into two discernable phases. These two phases have equal amplitudes when the fast direction of anisotropic layer orients N45°E. When the delay time is less than 1/4 period, two projections overlap and appear as a broadened phase.

[19] For the synthetic SKS seismograms displayed in Figure 5a, the SC method was employed to determine splitting parameters, the fast polarization direction ϕ, and delay time δt, assuming that SKS waves traverse a single homogeneous anisotropic layer. By minimizing the energy on the reconstructed transverse component, the best fitting ϕ and δt, from a grid search over trial ϕ and δt, were obtained. As a result, all shear wave splitting measurements with their 2σ uncertainty determined from the 95% confidence interval in the $\phi-\delta t$ domain are displayed in Figure 5b. The comparison shows that the calculated fast polarization directions are in excellent agreement with those of the designed model. The delay times, on the other hand, are in general slightly larger than the theoretical delay times which are obtained assuming vertical plane wave propaga-

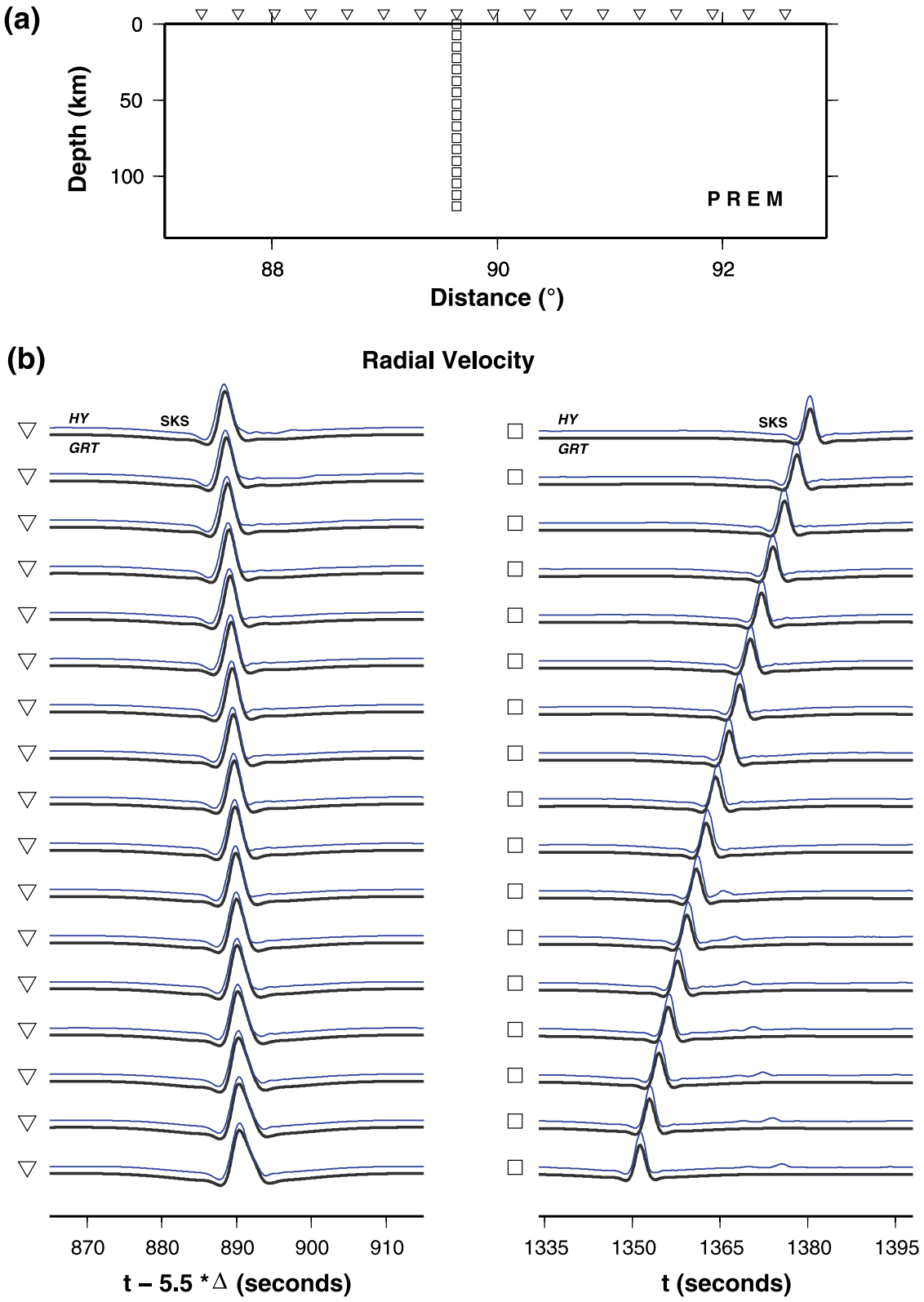

Figure 2. (a) PREM used for the calculations in which the Earth flattening approximation is applied; the triangles and squares mark the receivers. (b) Comparison of horizontal velocities obtained by the generalized ray theory (heavy traces) and the hybrid method (light traces) with a source depth of 131 km. All seismograms are plotted to the same scale.

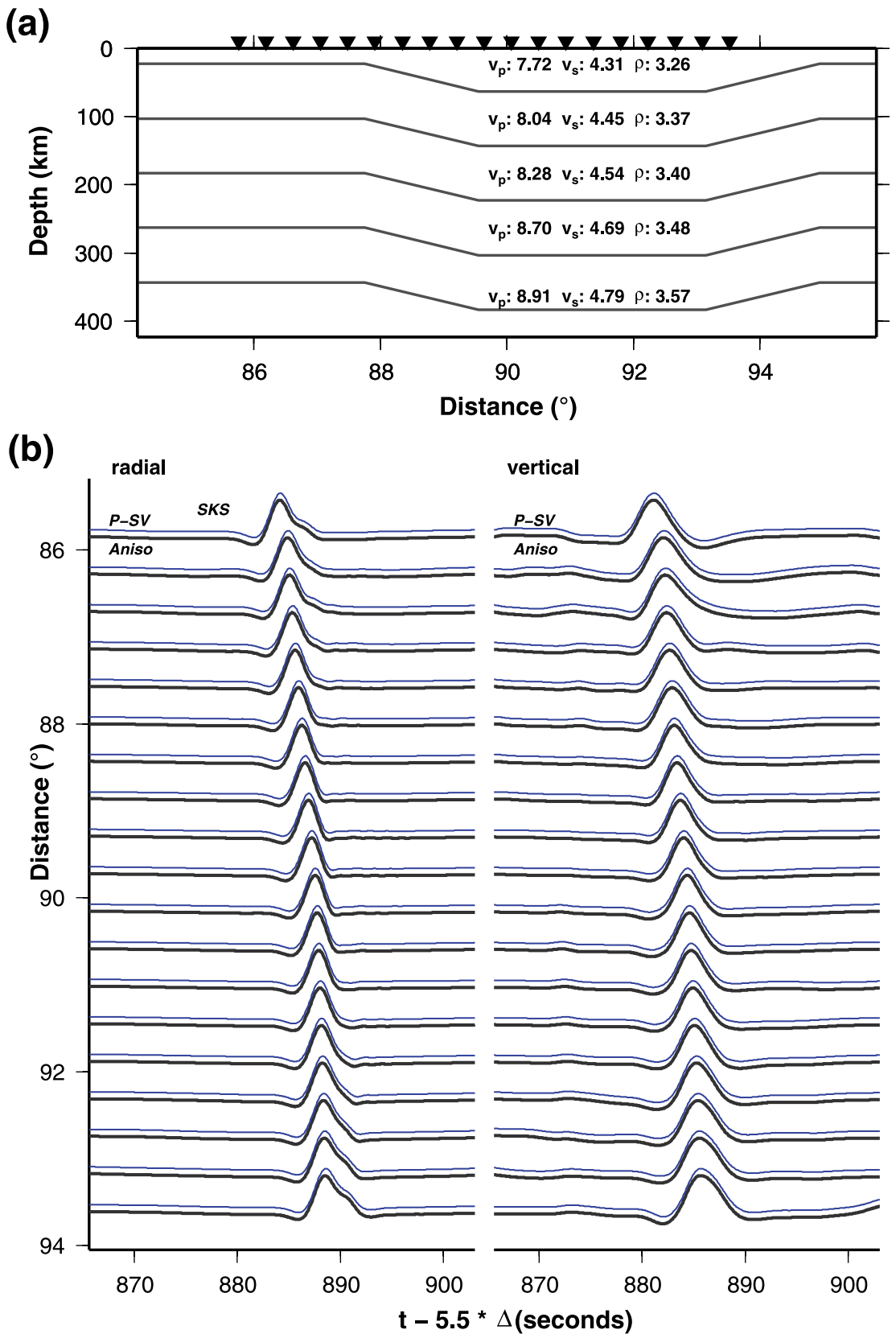

Figure 3. (a) Laterally varying isotropic model where finite difference is applied. PREM is used for outside GRT calculation. The triangles represent receivers. (b) Comparison of radial and vertical velocities obtained by the new method (heavy traces) and a P-SV method (light traces) by *Wen and Helmberger* [1998a]. All seismograms are plotted to the same scale. For displaying purpose, heavy traces are shifted away from their epicentral distances.

Table 1. Elastic Constants of Transversely Anisotropic Medium[a]

Constant	Value
c_{11}	260.78
c_{12}	80.00
c_{13}	80.00
c_{22}	200.77
c_{23}	72.99
c_{33}	72.99
c_{44}	63.89
c_{55}	72.90
c_{66}	72.90

[a]Density is 3.31 g/cm^3. See *Keith and Crampin* [1977b].

tion. This observation is consistent with the slightly oblique incidence of SKS at the epicenter distance considered. The slightly oblique incidence results in longer raypaths of the shear waves in the anisotropic layer and therefore larger time differences between the split waves than the case of vertical incidence. Also note that the observed time difference exhibits variations as the fast direction of the medium changes, indicating the SC method has less accuracy in measuring the delay times than in inferring the fast polarization directions.

4. Synthetics Calculations and Discussions on Some Representative Models

[20] Lateral variations in anisotropy appear to be ubiquitous in the Earth [*Savage*, 1999], because of complex geological and geodynamic processes in the Earth's history. In this section, we test several anisotropic structures they may be present in the Earth. They include (1) laterally varying anisotropic lithosphere, which may occur in the continental collision zone, (2) multilayer anisotropy, which may be related to a lithosphere overlying an asthenosphere, (3) large-scale separated anisotropic bodies, which may be related to lithospheric delamination, and (4) anisotropic models in the subduction zones. We performed several synthetical calculations to understand wave propagation through the complex anisotropic structures mentioned above. In all the models presented below, the elastic parameters for the transversely isotropic media given by *Keith and Crampin* [1977b] were adopted and listed in Table 1. Unless indicated otherwise, the calculated synthetics are band-pass filtered between 0.02 and 0.20 Hz.

4.1. Laterally Varying Anisotropic Models

[21] A laterally varying anisotropic structure may exist across a plate boundary between two plates. In this experiment, we designed a laterally varying anisotropic structure at the shallow depth, with two anisotropic domains in contact with each other. Without loss of generality, the designed model exhibits horizontal *a* axis orientations of N30°E for distances less than 89.55° and of N120°E for the larger distances (Figure 7a). The receivers, with a spacing of 12 km, are placed at the surface across the plate boundary.

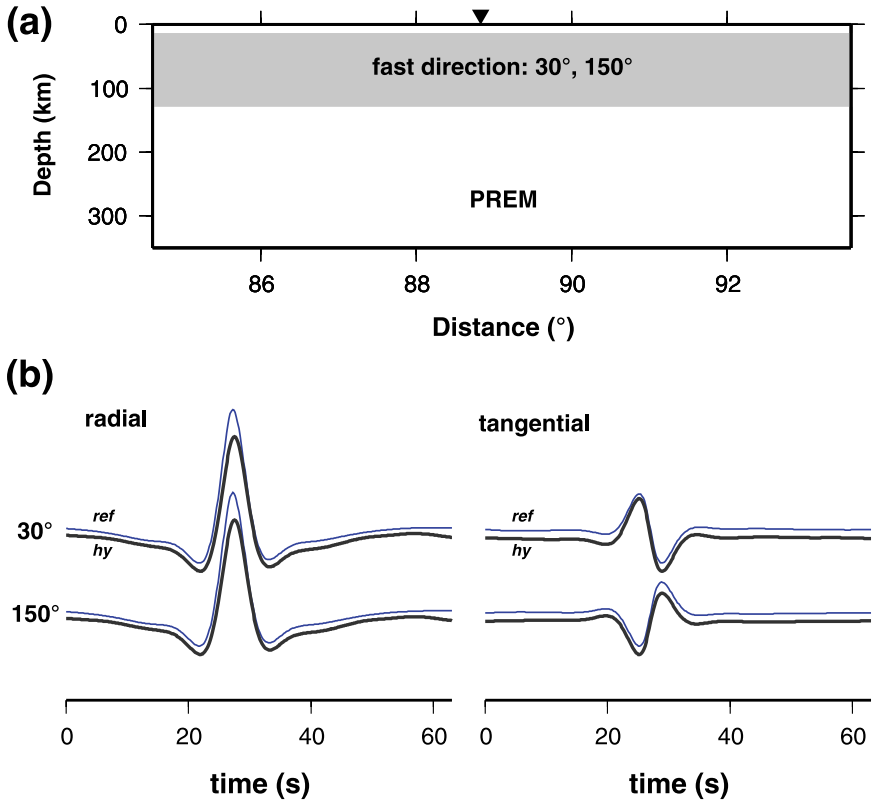

Figure 4. (a) An anisotropic layer embedded within the PREM with fast directions trending N30° and N150°. The triangle represents the receiver location where synthetics are calculated. (b) Comparison of horizontal velocities obtained by the one-dimensional anisotropic reflectivity method developed by *Keith and Crampin* [1977a, 1977b] (light traces) and the hybrid method (heavy traces). The synthetics are band-pass filtered between 0.02 and 0.125 Hz.

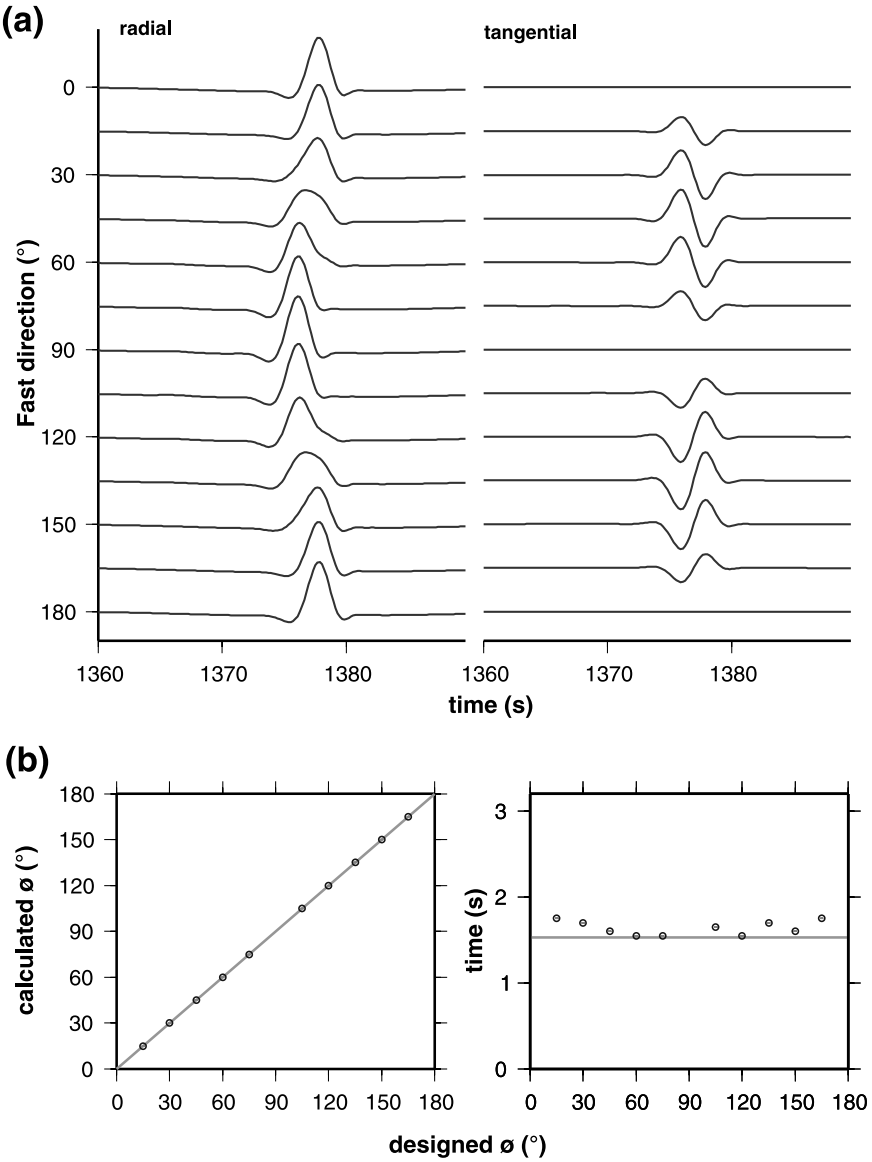

Figure 5. (a) Horizontal velocity synthetics in the (left) radial and (right) tangential directions calculated by the new method, for models with the fast direction of the anisotropic medium assumed various directions from 0° (top trace) to 180° (bottom trace). The geometry of the models is the same as that shown in Figure 4a. The synthetics are band-pass filtered between 0.02 and 0.20 Hz. (b) Splitting parameters (left) fast direction ϕ and (right) delay time δt calculated on the basis of the splitting analyses of the SKS synthetics using the SC method. The circle indicates the value; 2σ error bar is represented by thin gray line whose length is generally less than the diameter of circle; the gray line in Figure 5b (left) indicates the fast direction assumed for the anisotropic medium in the models, while that in Figure 5b (right) indicates the delay time between the fast and slow directions for an SKS wave vertically propagating through the models.

[22] Figures 7b, 7d, and 7e show surface motion and snapshots of horizontal wavefield due to an SKS incidence. The two quasi-shear waves ($x_1$and x_2 components) in an anisotropic medium can also be written as qSV and qSH, respectively [*Keith and Crampin*, 1977a, 1977b]. The occurrence of qSH wave transmitted from an SKS wave at the bottom of the anisotropic layer can be clearly observed from the wavefield snapshots of the radial (qSV), and tangential (qSH) components in the FD domain (Figures 7d and 7e). The waveforms are highly sensitive to the anisotropic parameters of the media; note that the polarity of the tangential component (x_2) synthetics reverses as the wave propagates from one anisotropic unit to the other (Figure 7b). Moreover, the arrival time of SKS phase in the x_1 components also jumps abruptly across the boundary. For most epicentral distances, both the fast polarization directions and delay times inferred from the synthetics by using the SC method are in good agreement with those of obtained from the designed model (Figure 7c). However, in the boundary zone within a width of $\sim$ 50 km,

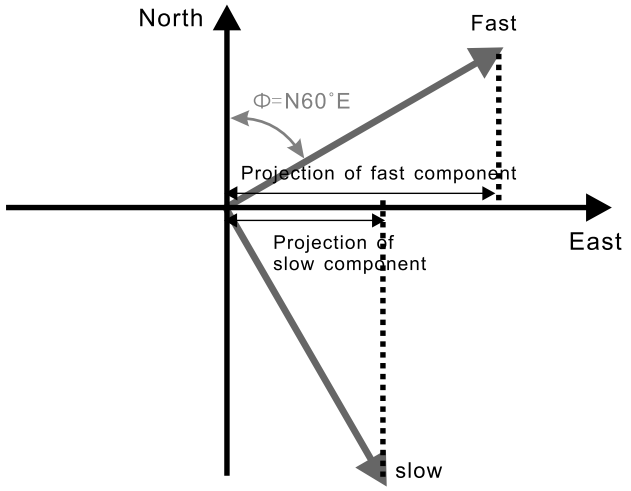

Figure 6. Schematic illustrating projection of fast and slow components onto the x_1 axis that introduces broadened or double phases (see text for details).

the fast polarization direction obtained from the SC method does not change as sharply as the anisotropic media. The fast direction gradually rotates from N60°E to N150°E across the boundary, indicating that it is difficult for the SC method to resolve the sharp feature between the two domains. In contrast, the sharp polarity reversal of the tangential component waveform (Figure 7b) suggests that the synthetic seismograms, if the dominant frequencies of the recorded waves permit, would have higher spatial resolution in constraining the boundary of the two anisotropic units. Rapid changes of the fast polarization direction were observed across the collisional boundary on the basis of the SC method. Some have argued, on the basis of the Fresnel zone analysis [e.g., *Rümpker and Ryberg*, 2000], the abrupt change of splitting parameters can be explained by the effects of anisotropic boundaries in the shallow depth. However, the above synthetics analyses suggest that caution is required to interpret the inferred abrupt change of the anisotropic parameters, even for the shallow anisotropic structures.

[23] To test the effects of the depth of the anisotropic layer, we modified the above laterally varying anisotropic model with the top boundary of the anisotropic layer deepened from 12 km to 76 km (Figure 8a), and changed the widths of the two anisotropic bodies to be 150 km, and then compared the synthetics and SKS splitting measurement results with those from the shallower anisotropy model. The transition zone of the splitting parameter variation inferred from the SC method broadens to ~96 km (Figure 8c). The deeper anisotropy model, however, still produces a rapid polarity reversal of the tangential component waveform across the boundary, although the position of the polarity reversal moves eastward (Figure 8b). The above synthetics tests indicate the higher sensitivity of waveform modeling for mapping deep sharp anisotropic structures.

4.2. Two-Layer Anisotropic Models

[24] We consider the propagation of SKS wave in two-layer anisotropic media. Two-layer anisotropic structure may result from an anisotropic lithosphere overlying an anisotropic asthenosphere or one lithosphere underplated beneath another during continental collisions [*Silver and Savage*, 1994]. In this experiment, we designed two series of models. In the first type of models (Figure 9a), we fixed the incoming SKS energy polarization to be parallel to east, and assumed an 80-km-thick asthenospheric layer with a fixed fast polarization direction of N45°E overlain by an 80-km-thick lithosphere with fast directions changing clockwise from north to south with an increment of 15°. Figure 9b shows the horizontal surface velocities. Figure 9c shows the splitting parameters calculated by the SC method. In general, the splitting parameters inferred from the synthetics by using the SC method show a π period with the fast direction of the top layer. The inferred apparent fast directions are intermediate to those of the overlying and underlying anisotropic layers. When the fast direction (from N30°E to N60°E) of the overlying layer is subparallel to that of the underlying layer, the radial components of SKS phases exhibit two discernible peaks with comparable amplitudes, and the tangential components possess the largest amplitude (Figure 9b). The double peaks in the radial component can be explained by energy projection, as discussed in section 3.3. When the fast direction of the overlying layer is perpendicular to that of the underlying layer, the tangential component displays small energy, which introduces large 2σ uncertainties in inferring the delay time on the basis of the SC method (Figure 9c).

[25] In the second type of models, we fixed the fast polarization directions of the two layers and changed the incoming SKS energy polarization direction from north to south by an increment of 10° (Figure 10a). We define the radial and tangential axes to be parallel and perpendicular to the incoming SKS energy direction, respectively. The apparent splitting parameters calculated by the SC method exhibit functions of incoming polarization direction with an approximately $\pi/2$ period (Figure 10c), in good agreement with the results of *Silver and Savage* [1994]. However, each pair of synthetics for one model parameter are different from the others in arrival time, polarity, waveform, and amplitude ratio between the radial and tangential components (Figure 10b), suggesting high sensitivity of waveform to model parameters.

Figure 7. (a) A 2-D anisotropic model embedded within the PREM. The anisotropic layer is divided into two parts with different *a* axis orientation. (b) Horizontal velocity synthetics produced by an SKS incident wave. The thick gray lines indicate the boundary between two anisotropic domains. (c) Splitting parameters (left) ϕ and (right) δt, calculated by the SC method. The circle indicates the value; gray line represents error bar. (d–e) Snapshots of the (left) radial and (right) tangential velocity wavefields of an SKS wave transmitted through the anisotropic model at t = 1345 s (Figure 7d) and t = 1360 s (Figure 7e). The thick gray line shows the boundary of the anisotropic layer.

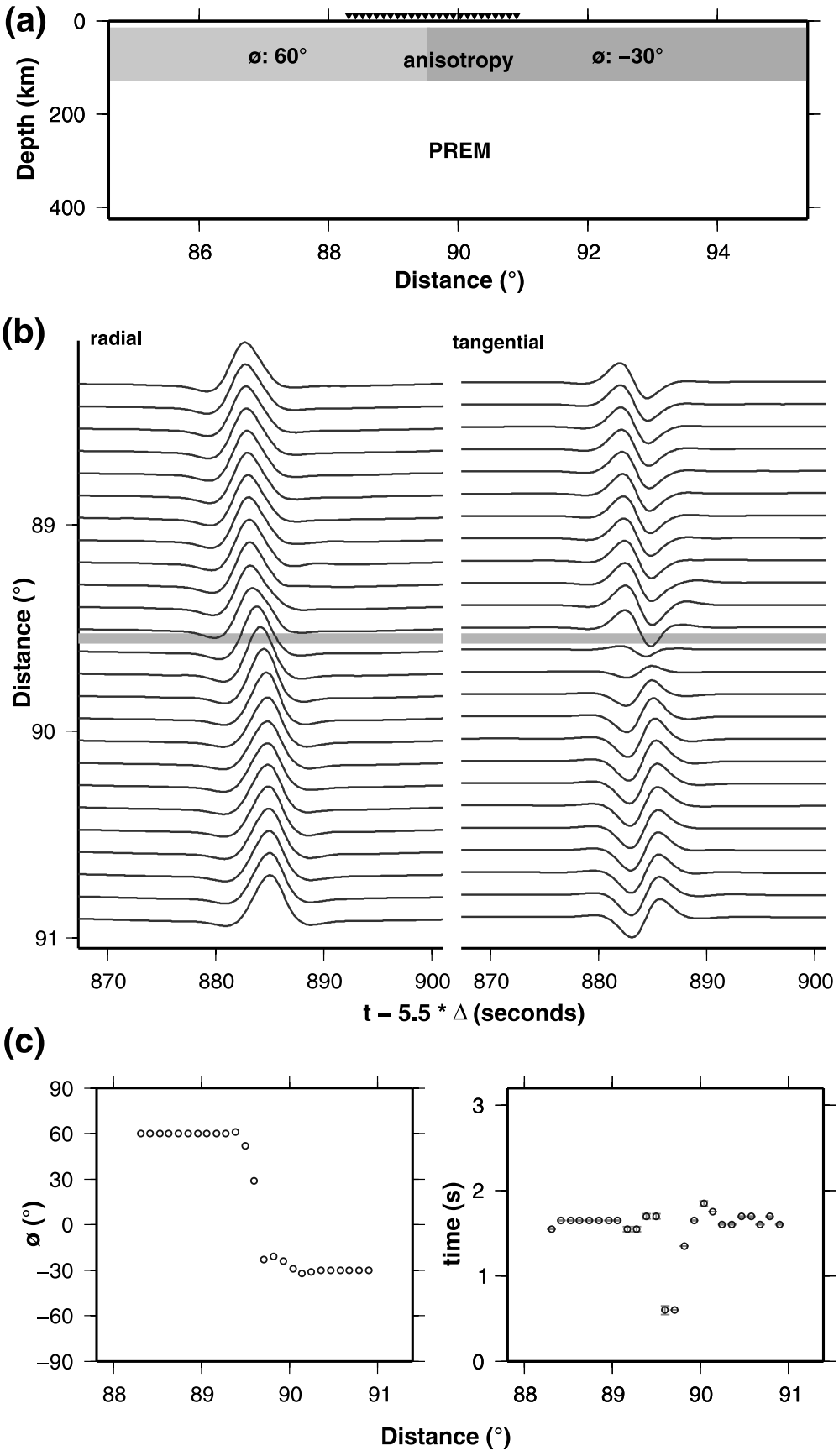
(a)
ø: 60°
anisotropy
ø: −30°
PREM
Depth (km)
Distance (°)
(b)
radial
tangential
Distance (°)
t – 5.5 * Δ (seconds)
(c)
ø (°)
time (s)
Distance (°)

Figure 7

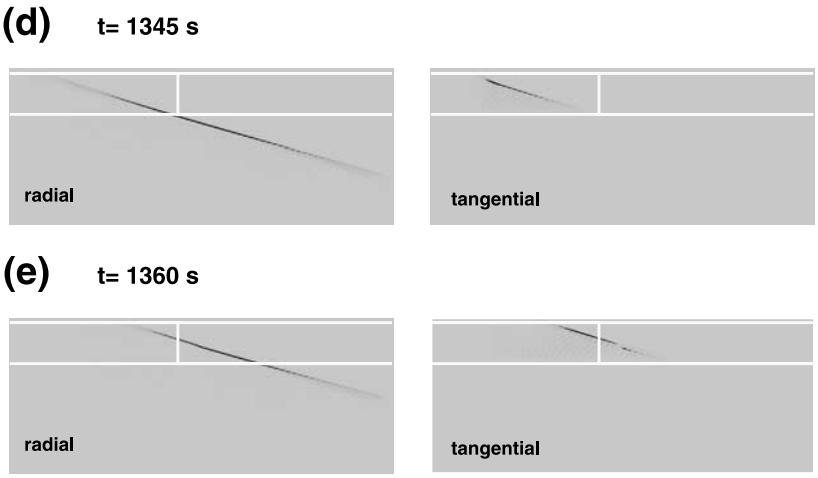

Figure 7. (continued)

4.3. Separated Anisotropic Body

[26] The gravity instability may introduce presence of a large-scale anisotropic delaminated lithosphere in the mantle. In this experiment, we designed a model with a 300-km-wide and 70-km-thick anisotropic body beneath the lithosphere (Figure 11a), representing a delaminated lithospheric block. We assumed h to represent the distance between the top of the delaminated block and the base of the overlying lithosphere. We changed h from 30 km to 120 km and calculated the synthetics. As an example, Figure 11b shows the horizontal velocity responses to the SKS wave incidence with h being equal to 120 km. Figure 11c presents the corresponding splitting parameters obtained by the SC method. For all the models with h from 30 km to 120 km, in the radial component, precursor energy is observed before the SKS phase for the receivers over the separated anisotropic body, while in the tangential component, only the broadened waveforms, but no precursor energy or discernible secondary phases, are observed.

[27] To test the effect of underlying anisotropic body on the precursor energy, we increased the thickness of the underlying anisotropic body to 110 km (Figure 12a) and calculated the corresponding synthetics. Figure 12b shows that the precursor energy of the SKS phases in radial component arrive $\sim$0.6 s earlier than that for the model with thinner underlying anisotropic body. These synthetics tests indicate that the precursor energy and the arrival time difference between the precursor energy and the SKS phase are related to the thickness and depth of the underlying anisotropic body. This information can be used to constrain the lithospheric delamination model through modeling the SKS wave precursor.

4.4. Anisotropic Models in the Subduction Zones

[28] Subduction may produce a complex anisotropic structure with a combination of lithosphere collision, two anisotropic layers, a sloping anisotropic slab, and probably a separated anisotropic body. For the models we tested, we assumed that the descending lithosphere has a dipping angle of 18.4° relative to the x_1 axis, a thickness of 80 km, a fast polarization direction parallel to N60°E, and the overriding lithosphere has a thickness of 70 km, a fast polarization direction perpendicular to that of the descending lithosphere (Figure 13a). We assigned receivers across the subduction zones and calculated the surface motion with the new hybrid method. Figure 13b displays the horizontal surface velocity responses to the SKS incidence. Seismic waves sampling the subduction zone are strongly influenced by the integral effects of the two anisotropic layers. Orthogonal or subparallel fast directions of the subducting and overriding layers would reduce or enhance the recorded anisotropic amplitude, respectively. As Figure 13b shows, with increase of the length of SKS raypath within the overriding lithosphere, the amplitude of tangential component decreases to zero due to increasing contribution of anisotropy of the overriding layer. The amplitude of the tangential component increases gradually at larger distances with polarity reversed as the shear wave splitting is gradually dominated by the anisotropy of the overriding plate. In contrast, shear wave splitting parameters obtained using the SC method (Figure 13c) display a complex pattern of variation in which the fast direction and delay time change irregularly across the boundary, bearing no resemblance to the real anisotropic structure in the model. This analysis from this simple model suggests the difficulty of interpreting the splitting results obtained on the basis of the SC method across the subduction zones.

[29] To investigate the influence of dipping angle of the descending lithosphere on the synthetics, we designed a similar subduction model, but with a larger dipping angle of 35.0° (Figure 14a). Figures 14b and 14c display the corresponding horizontal velocity responses and splitting results for the same receivers. These results exhibit similar characteristics as those in Figure 13, except that the changes of waveform and splitting parameters occur in a shorter distance range.

[30] During the subduction process, the breakdown of subducting slab would result in a separated anisotropic body in the mantle. In order to illustrate the interaction between the SKS incidence and the complex anisotropic structure, we designed a more complex model by combining the subduction model and a scattering body (Figure 15a). Figure 15b presents the corresponding horizontal velocity responses, and Figure 15c shows the splitting parameters.

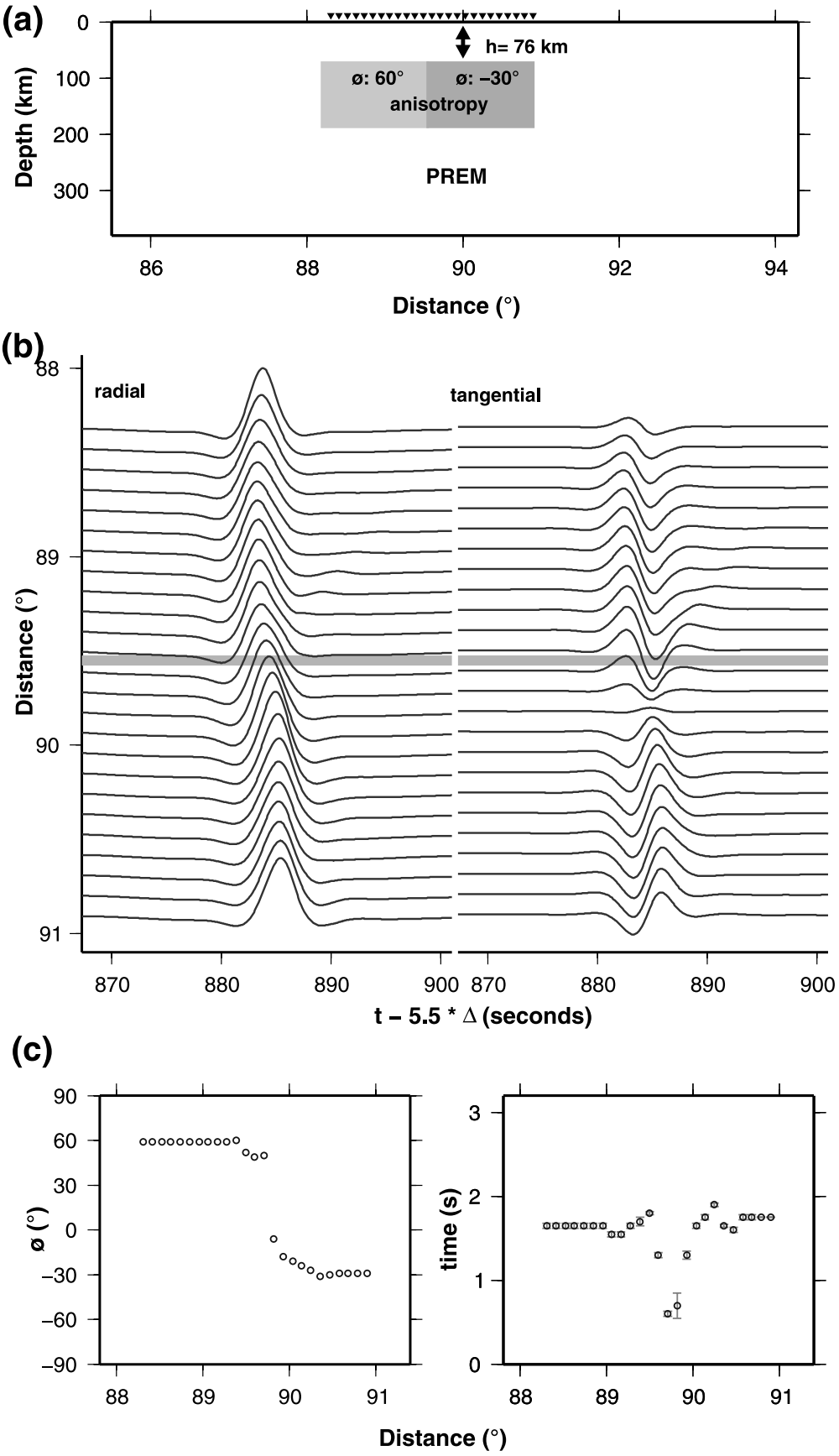

Figure 8. Same as Figures 7a–7c except that the top of the anisotropic layer extends to a depth of 76 km and the widths of the two anisotropic bodies are changed to 150 km.

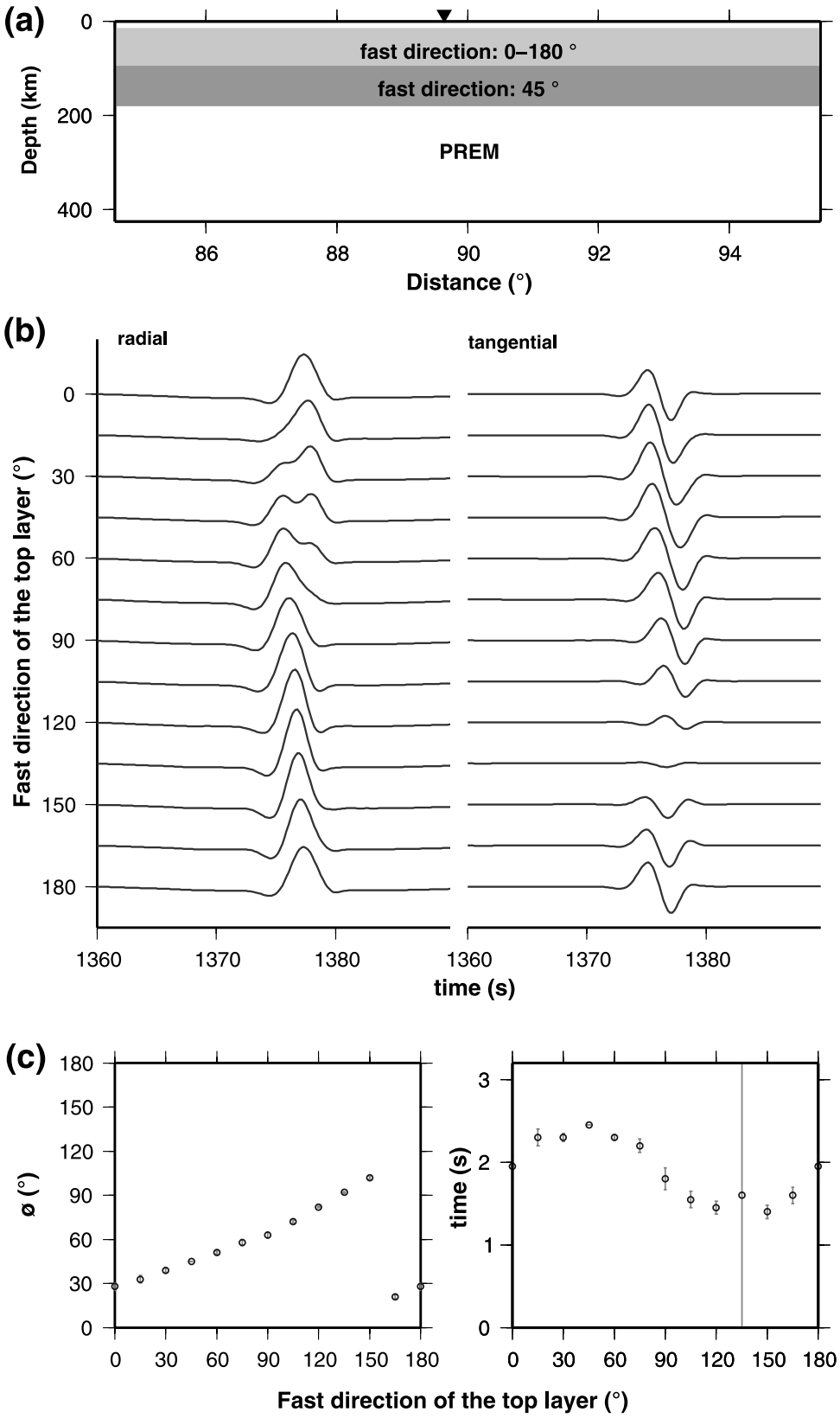

Figure 9. (a) Model with two anisotropic layers. The fast direction of anisotropy in the overlain layer orients N45°E, while that of the overlying layer changes from north to south with an increment of 15°. The triangle represents the receiver location where synthetics are calculated. (b) Horizontal velocities for different models. Vertical axis represents the fast direction of the overlying layer. The synthetics are band-pass filtered between 0.02 and 0.30 Hz. (c) Splitting parameters (left) ϕ and (right) δt calculated by the SC method. The circle indicates the value; error bar is represented by thin line.

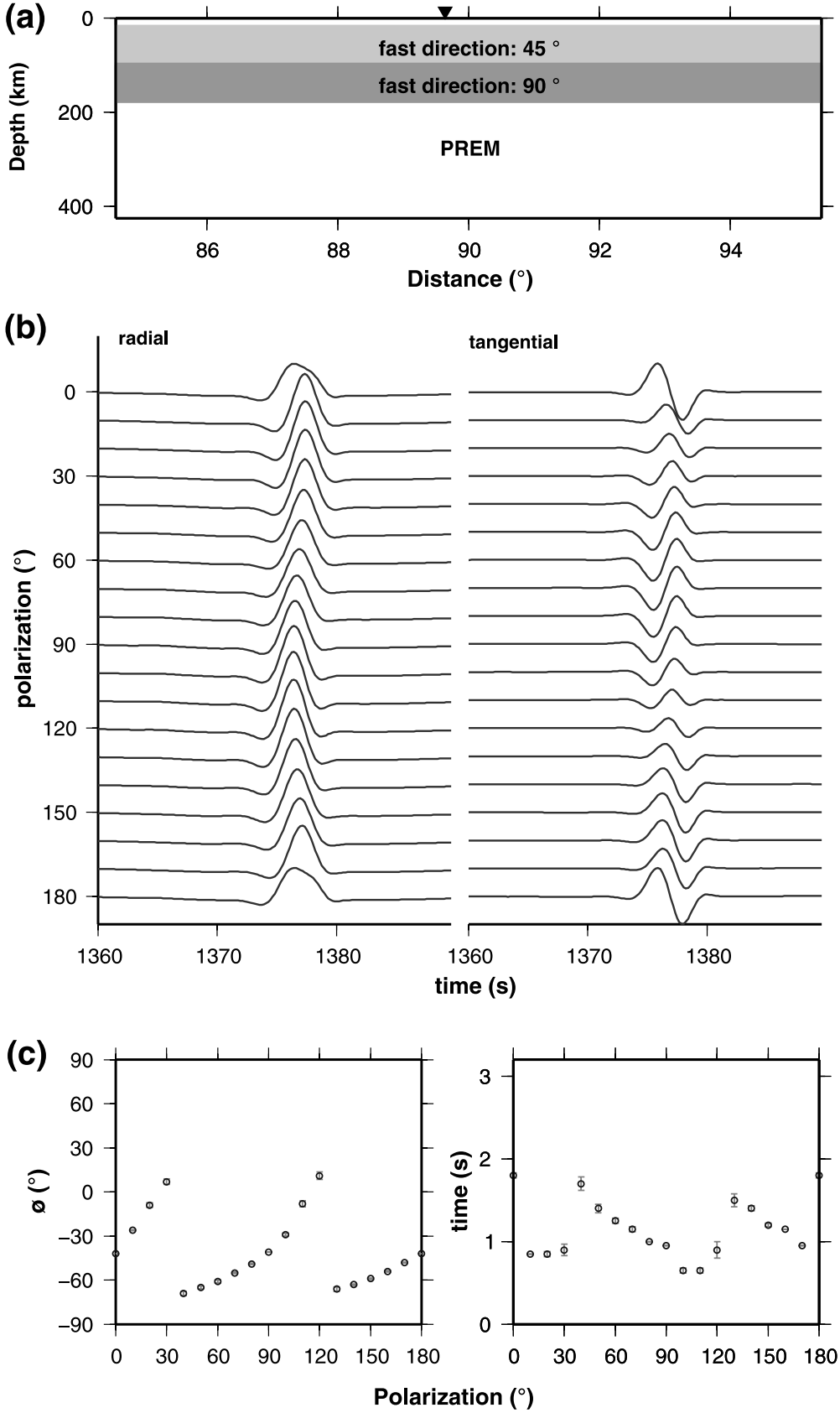

Figure 10. Same as Figure 9 except that the fast directions of two anisotropic layers are fixed and the incoming energy polarization is rotated from north to south.

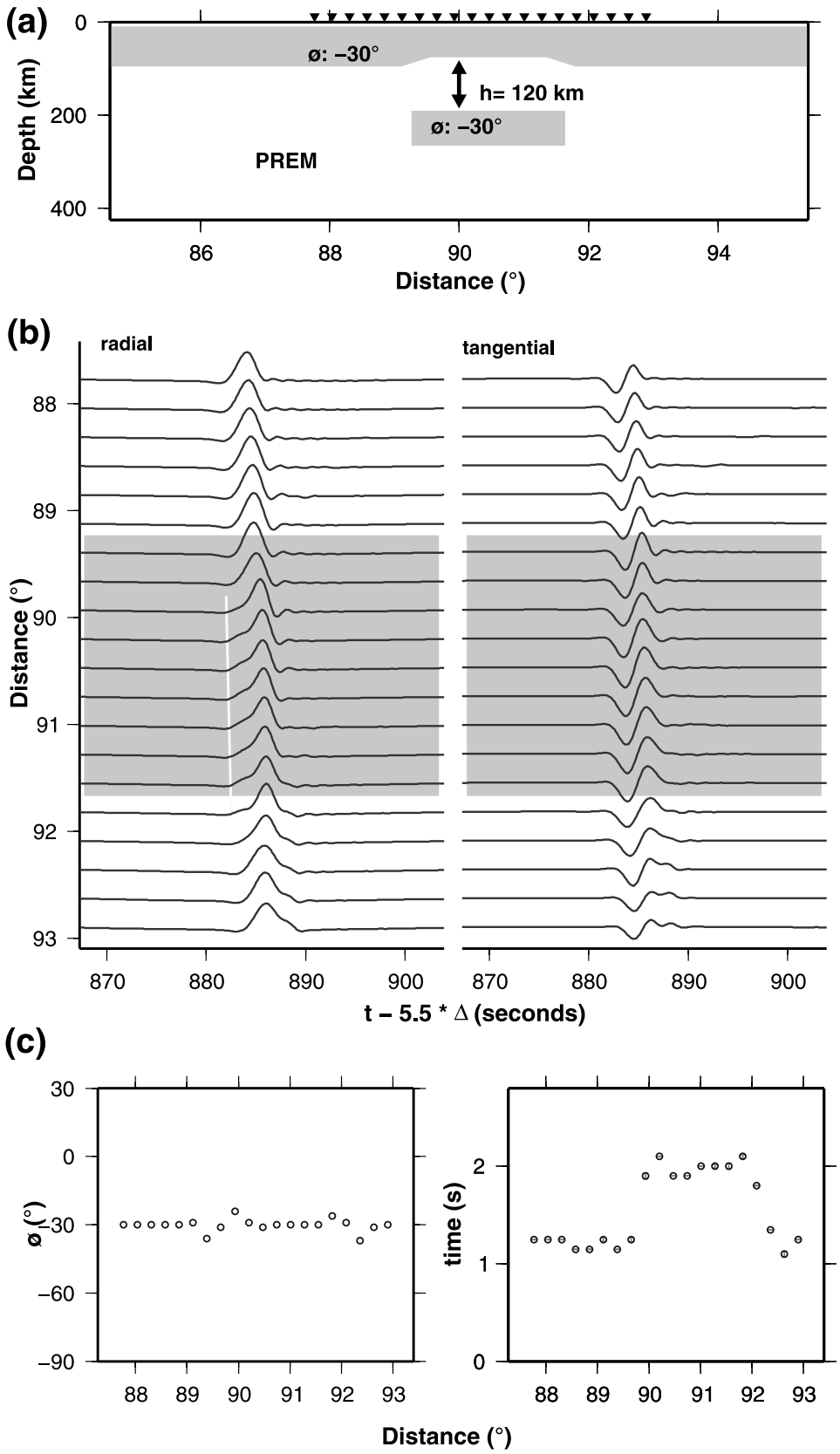

Figure 11. (a) Model with an underlying separated anisotropic body. The triangles represent receivers. (b) Horizontal velocities recorded at the surface. The synthetics are band-pass filtered between 0.02 and 0.30 Hz. The hatched distance range indicates region where the delaminated anisotropic body is located beneath. The white line marks the onset of precursor energy in radial component. (c) Splitting parameters (left) ϕ and (right) δt.

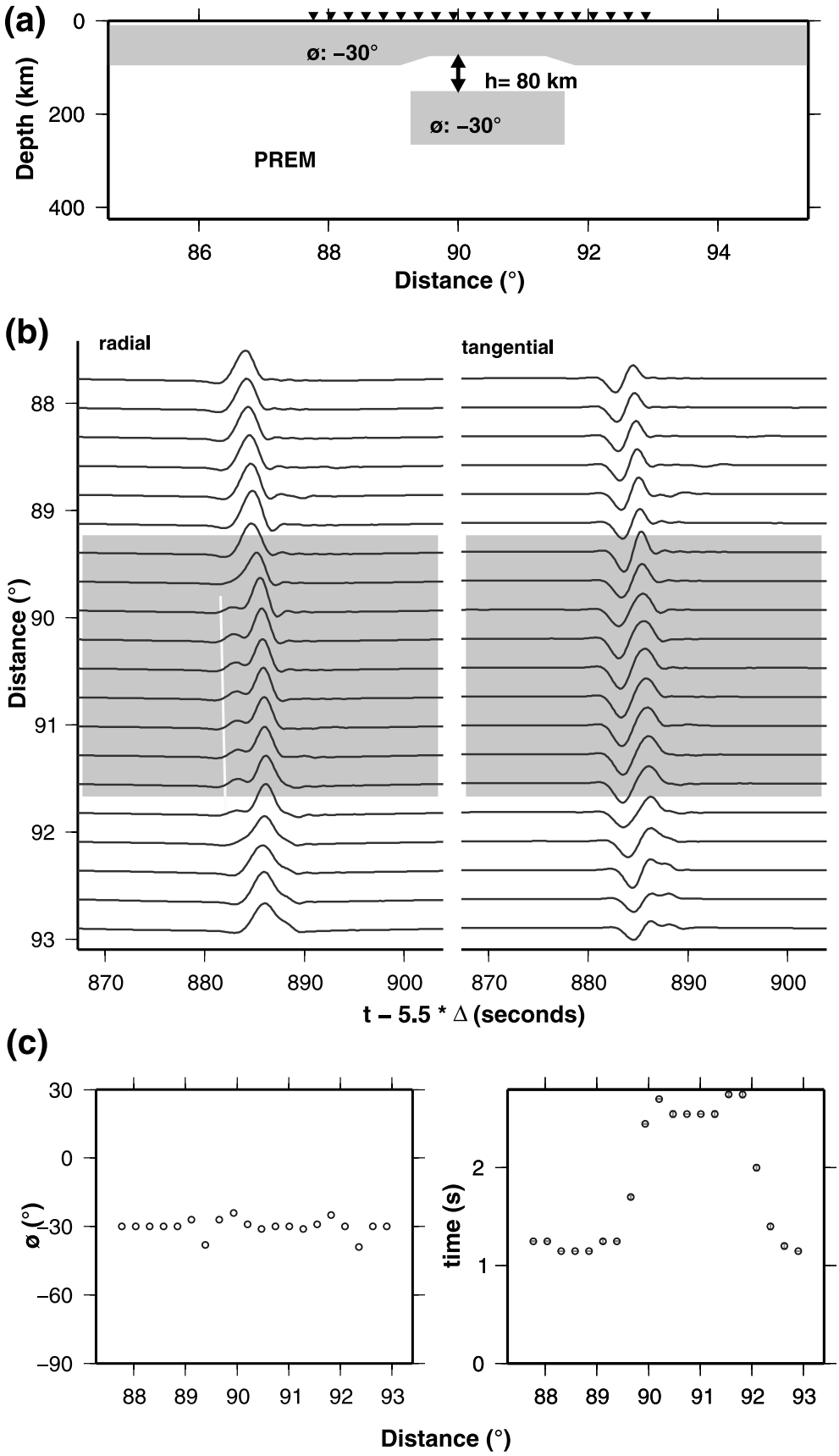

Figure 12. Same as Figure 11 except that the underlying anisotropic body is thickened from 70 km to 110 km. Note that the precursor energy of SKS phases in x_1 components arrives earlier than in Figure 11.

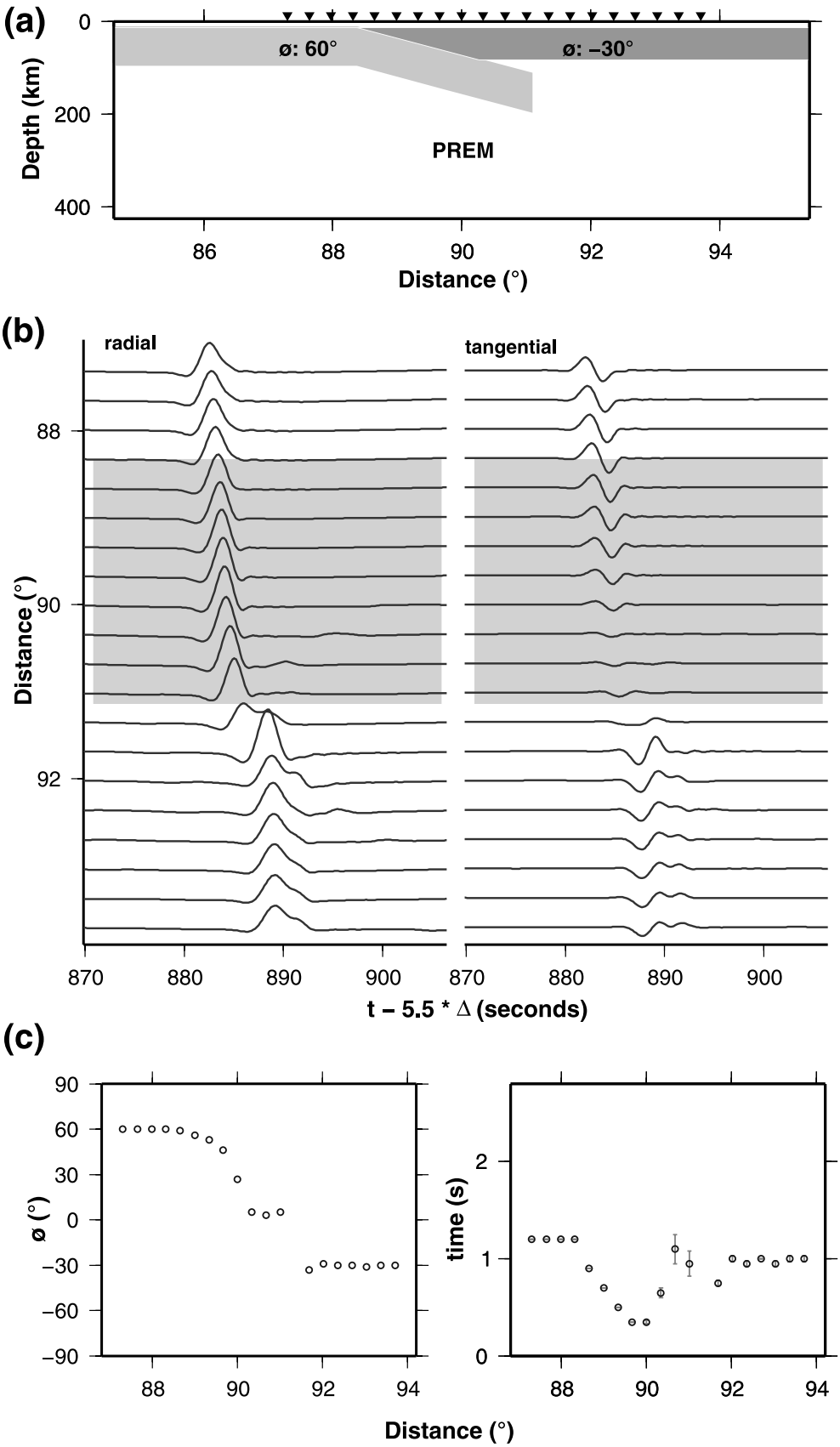

Figure 13. (a) Model of a subduction zone with an anisotropic plate descending beneath another plate with a different *a* axis of anisotropy. (b) Horizontal velocity synthetics recorded at the surface. The synthetics are band-pass filtered between 0.02 and 0.30 Hz. The hatched distance range indicates region where subduction occurred beneath. (c) Splitting parameters (left) ϕ and (right) δt.

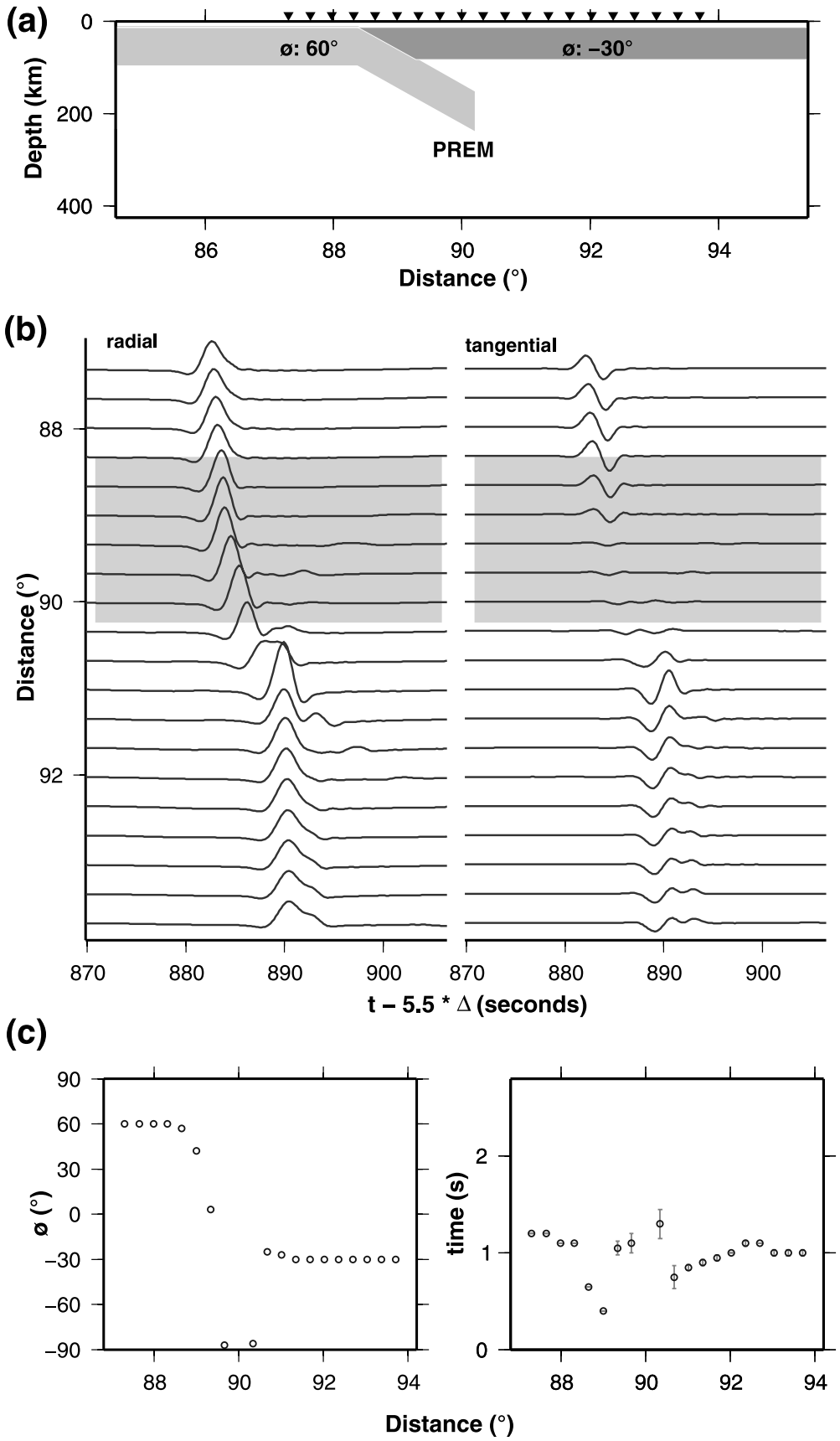

Figure 14. Same as Figure 13 except that the dipping angle of the descending lithosphere is changed from 18.4° to 35.0° relative to the x_1 axis.

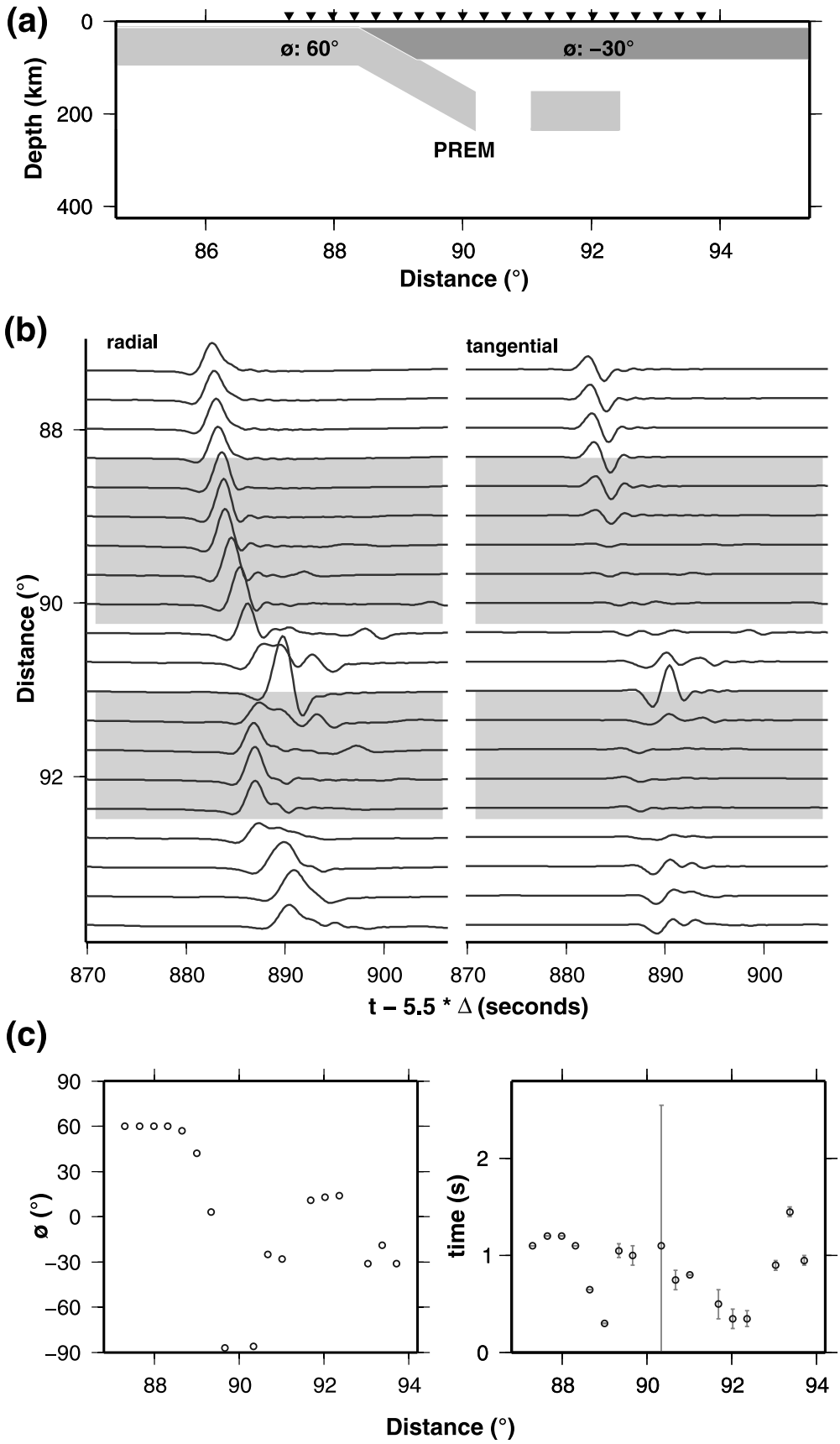

Figure 15. (a), (b), and (c) Same as Figure 13 except that a separated anisotropic body exists beneath the lithosphere. (d–f) Snapshots of the velocity wavefields at three time steps for the (left) radial and (right) tangential components, respectively.

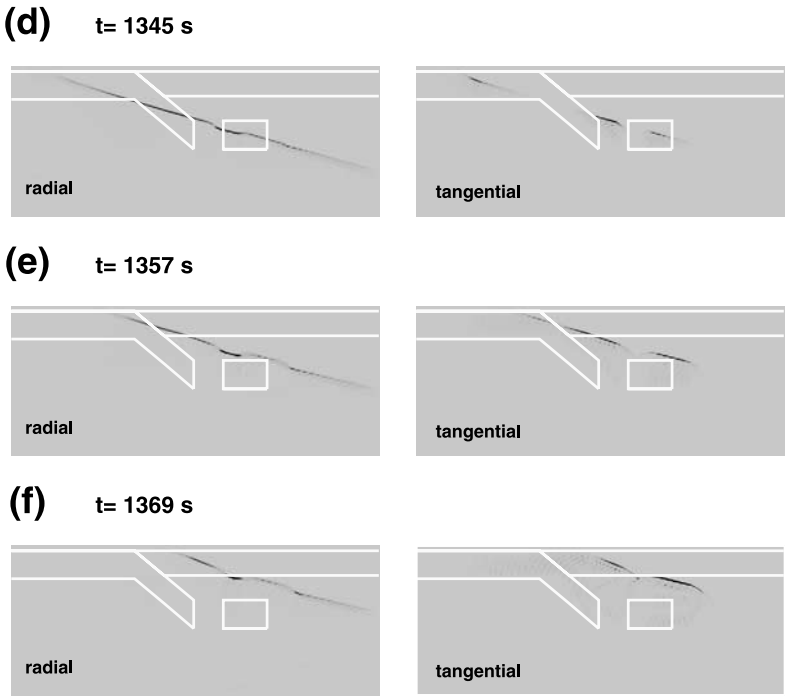

Figure 15. (continued)

The SKS wave propagation becomes more complex, and the SKS waveforms changed more rapidly in both the radial and tangential components. A series of snapshots of SKS wave propagation (Figures 15d, 15e, and 15f) through this model show that scattered energy is produced at the place where anisotropic property changes. Double or broadened phases, amplitude change of the radial and tangential components and polarity reversal of the tangential component are clearly observed across the subduction boundary (Figure 15b). The waveform information can be used to constrain the subduction model through modeling the SKS wave records. However, the splitting results obtained from the SC method become very difficult to interpret and are of limited use for inferring the anisotropy property beneath the receivers (Figure 15c).

5. Conclusion

[31] A two-dimensional hybrid method is developed for calculating synthetic seismograms for localized heterogeneous anisotropic structures. The hybrid method is a combination of analytic and numerical methods, with the finite difference technique applied in the laterally varying anisotropic region only and the analytic generalized ray method outside. Because the anisotropic region where the finite difference technique is applied has a smaller dimension compared with the spatial scale of teleseismic wave propagation, the hybrid method takes much less computer memory and time than the all-in-one numerical calculations and thus has wide applications in high-resolution studies of localized anisotropic structures. Comparison of synthetics calculated by this new method, GRT [*Helmberger*, 1983], a P-SV method [*Wen and Helmberger*, 1998a] and the one-dimensional anisotropic reflectivity method [*Keith and Crampin*, 1977a, 1977b] yield good agreements for isotropic models, respectively. Using the SC method, the extracted SKS splitting parameters for our synthetics are also in good agreement with those of the designed models. All the above tests verified the validity of the new hybrid method.

[32] We applied the hybrid method to study the SKS wave propagation problems in the anisotropic upper mantle. We calculated the synthetics for a series of laterally varying anisotropic models in the cases of lithosphere collision, two-layer anisotropy, lithospheric delamination, and subduction zones. Forward calculation provides a more physical approach for understanding the interaction between the seismic wave propagation and the anisotropic media. For the complex models, waveforms exhibit higher sensitivity to the spatial variation of anisotropy than the shear wave splitting parameters. With these advantages, this new hybrid method can be widely applied to constrain the anisotropic structures of the Earth. Besides the upper mantle, this method could also be used to study the anisotropic structures in other portions of the earth's interior after appropriate extension.

[33] **Acknowledgments.** We thank C. Cheng for his assistance. We also thank Editor J.C. Mutter, V. Levin, an anonymous reviewer, and an Associated Editor for constructive reviews. This research was financially supported by the National Science Foundation of China (40504006, 40434012, 90814002), an NSF grant EAR-0609717, and Chinese Academy of Sciences.

References

Booth, D. C., and S. Crampin (1983), The anisotropic reflectivity technique: anomalous reflected arrivals from an anisotropic upper mantle, *Geophys. J. R. Astron. Soc.*, *72*, 767–782.

Chen, L., L. Wen, and T. Zheng (2005), A wave equation migration method for receiver function imaging: 2. Application to the Japan subduction zone, *J. Geophys. Res.*, *110*, B11310, doi:10.1029/2005JB003666.

Chevrot, S. (2000), Multichannel analysis of shear wave splitting, *J. Geophys. Res.*, *105*, 21,579–21,590, doi:10.1029/2000JB900199.

Chevrot, S., N. Favier, and D. Komatitsch (2004), Shear wave splitting in three-dimensional anisotropic media, *Geophys. J. Int.*, *159*, 711–720, doi:10.1111/j.1365-246X.2004.02432.x.

Clayton, R., and B. Engquist (1977), Absorbing boundary conditions for acoustic and elastic wave equations, *Bull. Seismol. Soc. Am.*, *67*, 1529–1540.

Dziewonski, A., and D. L. Anderson (1981), Preliminary reference Earth model, *Phys. Earth Planet. Inter.*, *25*, 297–356, doi:10.1016/0031-9201(81)90046-7.

Hartog, R., and S. Y. Schwartz (2000), Subduction-induced strain in the upper mantle east of the Mendocino triple junction, California, *J. Geophys. Res.*, *105*, 7909–7930, doi:10.1029/1999JB900422.

Helmberger, D. V. (1983), Theory and application of synthetic seismograms, in *Earthquakes: Observation, Theory and Interpretation*, edited by H. Kanamori, pp. 173–222, Soc. Ital. di Fis., Bologna.

Huang, W. C., et al. (2000), Seismic polarization anisotropy beneath the central Tibetan Plateau, *J. Geophys. Res.*, *105*, 27,979–27,989, doi:10.1029/2000JB900339.

Igel, H., P. Mora, and B. Riollet (1995), Anisotropic wave propagation through finite-difference grids, *Geophysics*, *60*, 1203–1216, doi:10.1190/1.1443849.

Karato, S. (1987), Seismic anisotropy due to lattice preferred orientation of minerals: kinematic or dynamic?, in *High-Pressure Research in Mineral Physics*, *Geophys. Monogr. Ser.*, vol. 39, edited by M. H. Manghnani and S. Syono, pp. 455–471, AGU, Washington, D. C.

Keith, C. M., and S. Crampin (1977a), Seismic body waves in anisotropic media: reflection and refraction at a plane interface, *Geophys. J. R. Astron. Soc.*, *49*, 181–208.

Keith, C. M., and S. Crampin (1977b), Seismic body waves in anisotropic media: synthetic seismograms, *Geophys. J. R. Astron. Soc.*, *49*, 225–243.

Komatitsch, D., C. Barnes, and J. Tromp (2000), Simulation of anisotropic wave propagation based upon a spectral element method, *Geophysics*, *65*, 1251–1260, doi:10.1190/1.1444816.

Levander, A. R. (1988), Fourth-order finite-difference P-SV seismograms, *Geophysics*, *53*, 1425–1436, doi:10.1190/1.1442422.

Long, M. D., M. V. de Hoop, and R. D. van der Hilst (2008), Wave-equation shear wave splitting tomography, *Geophys. J. Int.*, *172*, 311–330.

Mainprice, D., G. Barruol, and Ben B. Ismail (2000), The seismic anisotropy of the Earth's mantle: From single crystal to polycrystal, in *Earth's Deep Interior: Mineral Physics and Tomography From the Atomic to the Global Scale*, *Geophys. Monogr. Ser.*, vol. 117, edited by S.-I. Karato, pp. 237–264, AGU, Washington, D. C.

Musgrave, M. J. P. (1970), *Crystal Acoustics*, Holden-Day, San Francisco, Calif.

Niu, F., and A. M. Perez (2004), Seismic anisotropy in the lower mantle: A comparison of waveform splitting of SKS and SKKS, *Geophys. Res. Lett.*, *31*, L24612, doi:10.1029/2004GL021196.

Rümpker, G., and T. Ryberg (2000), New "Fresnel-zone" estimates for shear-wave splitting observations from finite-difference modeling, *Geophys. Res. Lett.*, *27*, 2005–2008, doi:10.1029/2000GL011423.

Rümpker, G., T. Ryberg, G. Bock, and the Desert Seismology Group (2003), Boundary-layer mantle flow under the Dead Sea transform fault inferred from seismic anisotropy, *Nature*, *425*, 497–501, doi:10.1038/nature01982.

Ryberg, T., M. Tittgemeyer, and F. Wenzel (2000), Finite difference modeling of elastic wave propagation in the Earth's uppermost mantle, in *High Performance Computing in Science and Engineering '99: Transactions of the High Performance Computing Center, Stuttgart (HLRS) 1999*, edited by E. Krause and W. Jäger, pp. 3–12, Srpinger, Berlin.

Salimbeni, S., S. Pondrelli, L. Margheriti, V. Levin, J. Park, J. Plomerova, and V. Babuska (2007), Abrupt change in mantle fabric across northern Apennines detected using seismic anisotropy, *Geophys. Res. Lett.*, *34*, L07308, doi:10.1029/2007GL029302.

Saltzer, R. L., J. B. Gaherty, and T. H. Jordan (2000), How are vertical shear wave splitting measurements affected by variations in the orientation of azimuthal anisotropy with depth, *Geophys. J. Int.*, *141*, 374–390, doi:10.1046/j.1365-246x.2000.00088.x.

Savage, M. K. (1999), Seismic anisotropy and mantle deformation: What have we learned from shear wave splitting?, *Rev. Geophys.*, *37*, 65–106, doi:10.1029/98RG02075.

Silver, P. G., and W. W. Chan (1991), Shear wave splitting and subcontinental mantle deformation, *J. Geophys. Res.*, *96*, 16,429–16,454, doi:10.1029/91JB00899.

Silver, P. G., and M. K. Savage (1994), The interpretation of shear-wave splitting parameters in the presence of two anisotropic layers, *Geophys. J. Int.*, *119*, 949–963, doi:10.1111/j.1365-246X.1994.tb04027.x.

Stead, R. J., and D. V. Helmberger (1988), Numerical-analytical interfacing in two dimensions with applications to modeling NTS seismograms, *Pure Appl. Geophys.*, *128*, 157–193, doi:10.1007/BF01772596.

Vinnik, L. P., V. Farra, and B. Romanowwicz (1989), Azimuthal anisotropy in the earth from observation of SKS at SCOPE and NARS broadband stations, *Bull. Seismol. Soc. Am.*, *79*, 1542–1558.

Virieux, J. (1984), SH-wave propagation in heterogeneous media: Velocity-stress finite-difference method, *Geophysics*, *49*, 1933–1957, doi:10.1190/1.1441605.

Virieux, J. (1986), P-SV wave propagation in heterogeneous media: velocity-stress finite-difference method, *Geophysics*, *51*, 889–901, doi:10.1190/1.1442147.

Wang, Y., and L. X. Wen (2007), Complex seismic anisotropy near the border of a very low velocity province at the base of the Earth's mantle, *J. Geophys. Res.*, *112*, B09305, doi:10.1029/2006JB004719.

Wen, L. (2002), An SH hybrid method and shear velocity structures in the lowermost mantle beneath the central Pacific and South Atlantic Oceans, *J. Geophys. Res.*, *107*(B3), 2055, doi:10.1029/2001JB000499.

Wen, L. X., and D. V. Helmberger (1998a), A two-dimensional P-SV hybrid method and its application to modeling localized structures near the core-mantle boundary, *J. Geophys. Res.*, *103*, 17,901–17,918, doi:10.1029/98JB01276.

Wen, L. X., and D. V. Helmberger (1998b), Ultra low velocity zones near the core mantle boundary from broadband PKP precursors, *Science*, *279*, 1701–1703, doi:10.1126/science.279.5357.1701.

Wen, L. X., and F. L. Niu (2002), Seismic velocity and attenuation structures in the top of the Earth's inner core, *J. Geophys. Res.*, *107*(B11), 2273, doi:10.1029/2001JB000170.

Yang, D. H., E. Liu, Z. J. Zhang, and J. Teng (2002), Finite-difference modeling in two-dimensional anisotropic media using a flux-corrected transport technique, *Geophys. J. Int.*, *148*, 320–328, doi:10.1046/j.0956-540x.2001.01575.x.

Zhang, S. Q., and S. I. Karato (1995), Lattice preferred orientation of olivine aggregates deformed in simple shear, *Nature*, *375*, 774–777, doi:10.1038/375774a0.

Zhao, L., and T. Y. Zheng (2005), Using shear wave splitting measurements to investigate the upper mantle anisotropy beneath the North China Craton: Distinct variation from east to west, *Geophys. Res. Lett.*, *32*, L10309, doi:10.1029/2005GL022585.

Zhao, L., L. X. Wen, L. Chen, and T. Y. Zheng (2006), A two-dimensional hybrid method for calculating seismograms for seismic waves propagating in anisotropic media and its application, *Eos Trans. AGU*, *8*(52), Fall Meet. Suppl., Abstract S53B-1138.

L. Chen, L. Zhao, and T. Zheng, Seismological Laboratory, Institute of Geology and Geophysics, Chinese Academy of Sciences, Beituchengxi Road 19, P.O. Box 9825, Beijing, 100029, China. (lchen@mail.igcas.ac.cn; zhaoliang@mail.igcas.ac.cn; tyzheng@mail.igcas.ac.cn)

L. Wen, Department of Geosciences, State University of New York at Stony Brook, Stony Brook, NY 11794-2100, USA. (lianxing.wen@sunysb.edu)